

## Supplementary Information

# Porphyrin–Nanodiamond Hybrid Materials—Active, Stable and Reusable Cyclohexene Oxidation Catalysts

Lucas D. Dias <sup>1,2,\*</sup>, Fábio M. S. Rodrigues <sup>1</sup>, Mário J. F. Calvete <sup>1</sup>, Sónia A. C. Carabineiro <sup>3,4,\*</sup>, Marisa D. Scherer <sup>5</sup>, Anderson R. L. Caires <sup>5,6</sup>, Josephus G. Buijnsters <sup>7</sup>, José L. Figueiredo <sup>3</sup>, Vanderlei S. Bagnato <sup>2,8</sup> and Mariette M. Pereira <sup>1,\*</sup>

<sup>1</sup> Departamento de Química, CQC, Universidade de Coimbra, Rua Larga, 3004-535, Coimbra, Portugal; fmsrodrigues.qui@gmail.com (F.M.S.R.); mcalvete@qui.uc.pt (M.J.F.C.)

<sup>2</sup> São Carlos Institute of Physics, University of São Paulo, 13566-590, São Carlos, Brazil; vander@ifsc.usp.br

<sup>3</sup> Laboratory of Catalysis and Materials, Associate Laboratory LSRE-LCM, Faculty of Engineering, University of Porto, Rua Dr. Roberto Frias s/n, 4200-465 Porto, Portugal; jlfig@fe.up.pt

<sup>4</sup> LAQV-REQUIMTE, Department of Chemistry, NOVA School of Science and Technology, Universidade NOVA de Lisboa, Quinta da Torre, 2829-516 Caparica, Portugal

<sup>5</sup> Grupo de Óptica e Fotônica, Universidade Federal de Mato Grosso do Sul, CP 549, 790070-900 Campo Grande, MS, Brazil; marisa\_bio\_scherer@hotmail.com (M.D.S.); anderson.caires@ufms.br (A.R.L.C.)

<sup>6</sup> School of Life Sciences, University of Essex, Colchester CO4 3SQ, United Kingdom

<sup>7</sup> Department of Precision and Microsystems Engineering, Micro and Nano Engineering, Delft University of Technology, 2628 CD Delft, The Netherlands; J.G.Buijnsters@tudelft.nl

<sup>8</sup> Hagler Fellow, Department of Biomedical Engineering, Texas A&M University–College Station Texas, 400 Bizzell St, College Station, TX 77843, USA

\* Correspondence: sonia.carabineiro@fct.unl.pt (S.A.C.C.); mmpereira@qui.uc.pt (M.M.P.); lucas.dias1@usp.br (L.D.D.); Tel.: +351-21294857 (S.A.C.C.); +351-239-852080 (M.M.P.); +55-16-3373-9810 (L.D.D.)

## Content

**Figure S1.** XPS results of hybrid sample ND@βNH-TPPpCF<sub>3</sub>-Cu(II): C1s (a,b), N1s (c), O1s (d), F1s (e), Cu 2p (f).

**Figure S2.** XPS results of hybrid sample ND@βNH-TPPpCF<sub>3</sub>: C1s (a,b), N1s (c), O1s (d), F1s (e).

**Figure S3.** Survey XPS spectra of ND@βNH-TPPpCF<sub>3</sub>-Cu(II) (a) and ND@βNH-TPPpCF<sub>3</sub> (b).

**Figure S4.** TG-DSC curves of: a) ND@NH<sub>2</sub>; b) ND@βNH-TPPpCF<sub>3</sub>-Cu(II); c) ND@βNH-TPPpCF<sub>3</sub>; weight loss (solid line); heat flow (dashed line)

**Figure S5.** Effect of the ND@NH<sub>2</sub>, ND@βNH-TPPpCF<sub>3</sub> and H<sub>2</sub>O (control group) on **a)** the germination index (GI); **b)** the root elongation index (REI); **c)** the mitotic index (MI); **d)** the micronucleus index (MNI); and **e)** the nuclear abnormality index (NAI) of the *A. cepa* cells. Data represent the mean ± standard error and different letters means significant difference among the groups (p < 0.05). *Allium cepa* seeds were exposed to three concentrations (10, 50 and 100 mg/L).

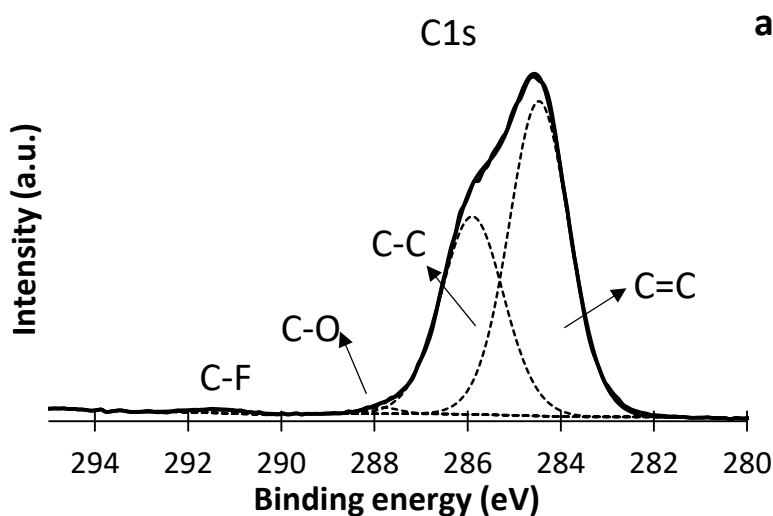
Figures S1a,b and S2a,b show the C1s spectra. The peak around 284 eV is attributed to  $sp^2$  carbon mainly related to ND surface [1,2], while the ~286 eV peak is typical of carbon ( $sp^3$ ) expected in diamond samples [2]. There is a small peak at ~288 eV (Figures S1b and S2b) attributed to C-O bonds [3]. Finally, another small peak can be found at ~292 eV (Figures S1b and S2b), which is often attributed to C-F bonds [4], thus due to the anchored complexes.

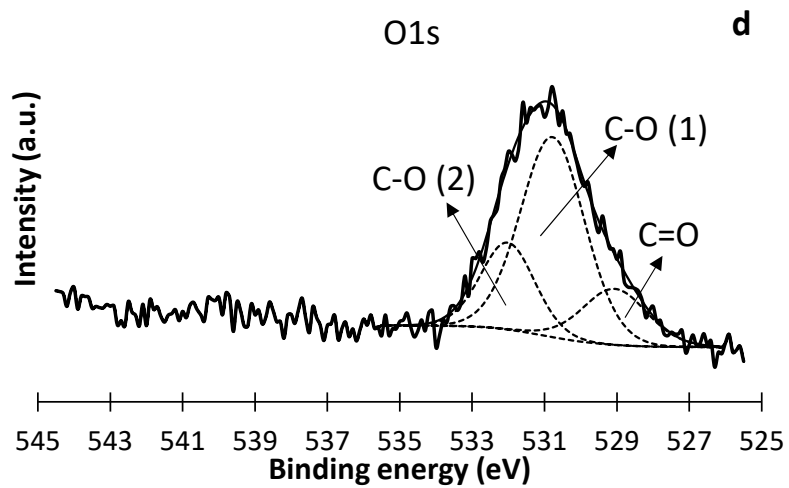
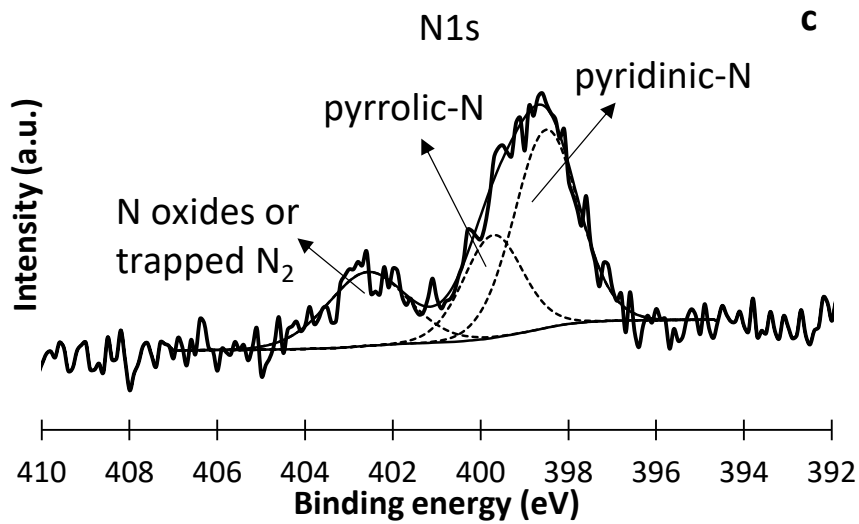
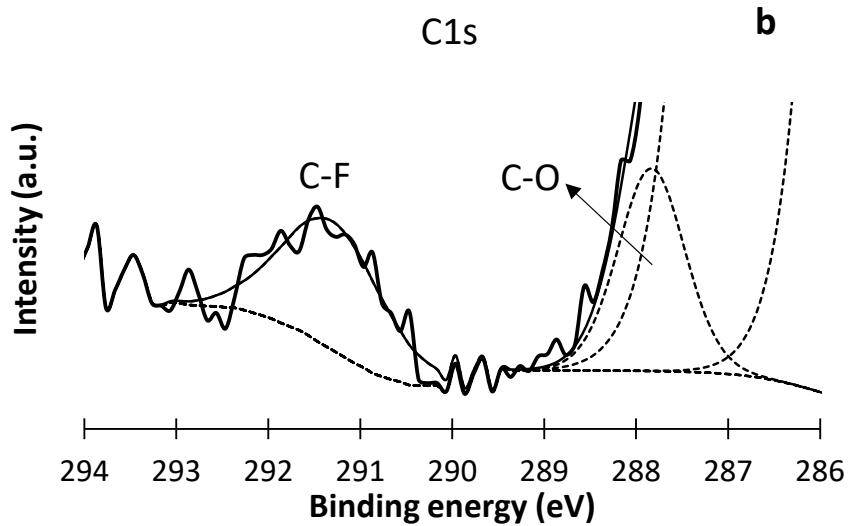
Figures S1c and S2c show three peaks in the N1s spectra. The first peak at ~399 eV is attributed to pyridinic-N groups, while the peak at ~400 eV is ascribed to pyrrolic-N groups [38]. The third peak at ~403 eV can be related to nitrogen trapped in the nanodiamond lattice [2] or N oxides [3]. The presence of nitrogen in NDs may be explained by the incorporation during the detonation synthesis [5]. The contribution from the anchored complex is not visible.

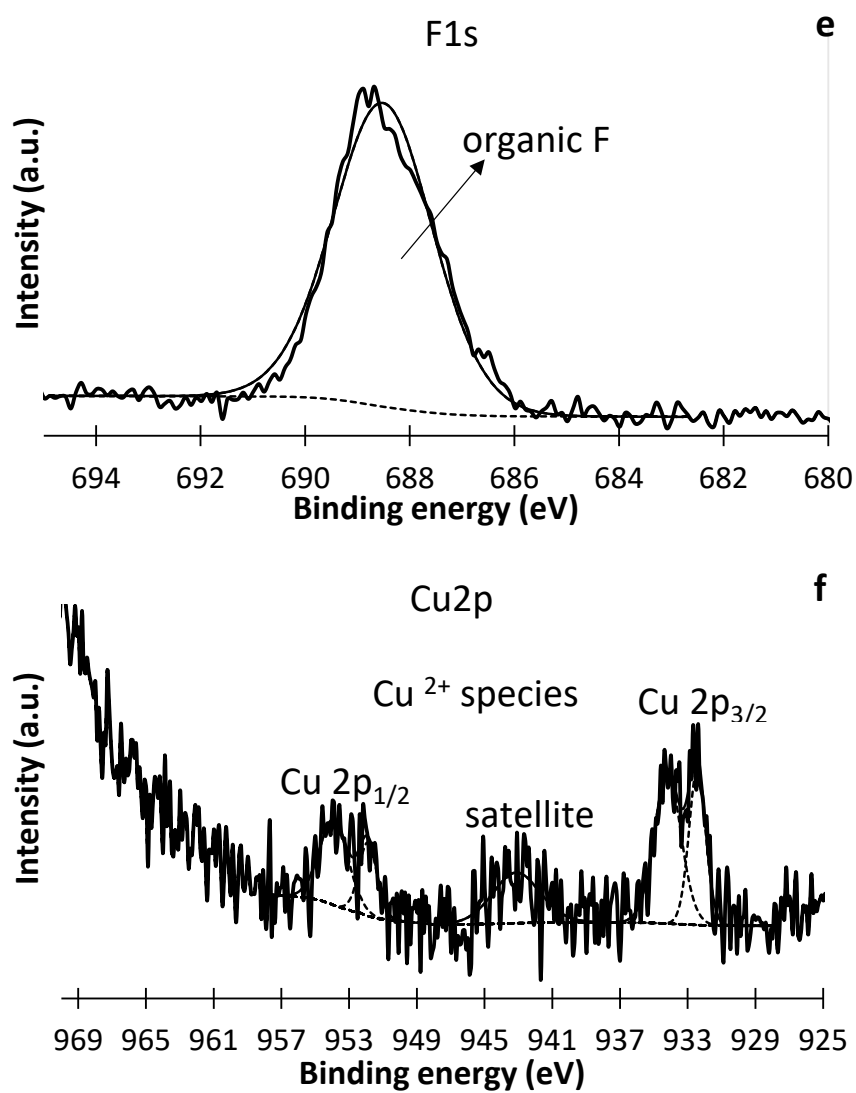
Figures S1d and S2d show that the O1s spectra can be deconvoluted to double-bonded oxygen (C=O), single-bonded oxygen in alcohol (OH), ether and/or epoxy groups C-O (1) and single-bonded oxygen (C-O) for carboxyl and ester groups (2), located at ~530 eV, ~531 eV and ~533 eV, respectively. The presence of double-bonded oxygen is expected in ND functionalized samples, due to oxygen containing carboxylic acid groups formed following acid treatments often used in the preparation of the pristine ND and the further treatment for surface functionalization, including amination [2].

Figures S1e and S2e show the presence of a single peak for F1s, at ~688 eV, characteristic of organic fluorine, confirming the presence of F in the samples [4].

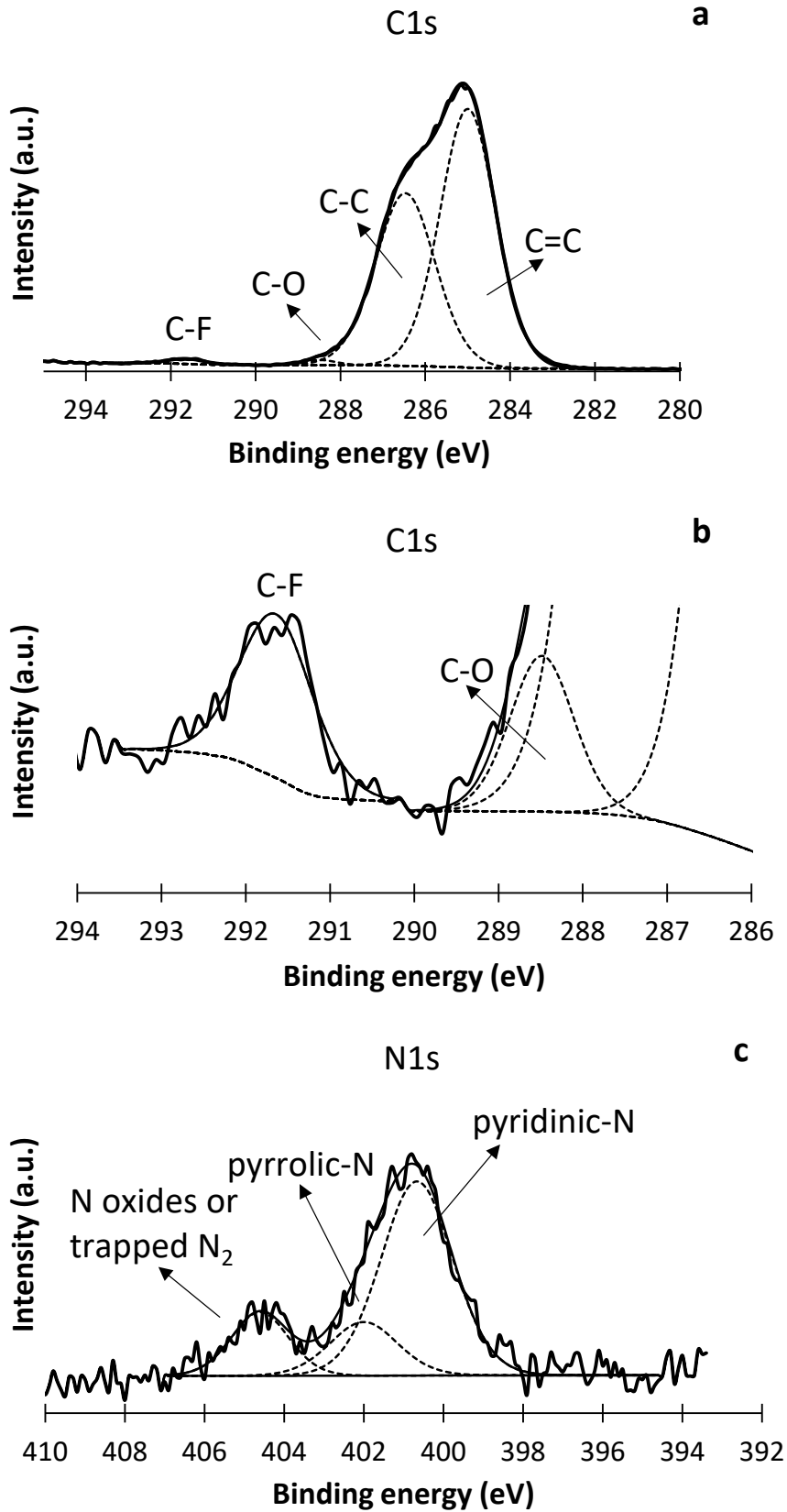
Figure S1f shows two peaks of Cu  $2p_{1/2}$  (~953 eV) and Cu  $2p_{3/2}$  (~933 eV), in addition to a shake-up satellite peak at 943 eV, which are typical for  $Cu^{2+}$  species [6], thus confirming the formation of the Cu(II)-based complex. It is worth noting that the C1s spectrum is much larger than that of the other elements, especially Cu 2p, which is in line with the amounts found for each element (Table 1).







**Figure S1.** XPS results of hybrid sample ND@ $\beta$ NH-TPPpCF<sub>3</sub>-Cu(II): C1s (a,b), N1s (c), O1s (d), F1s (e), Cu 2p (f).



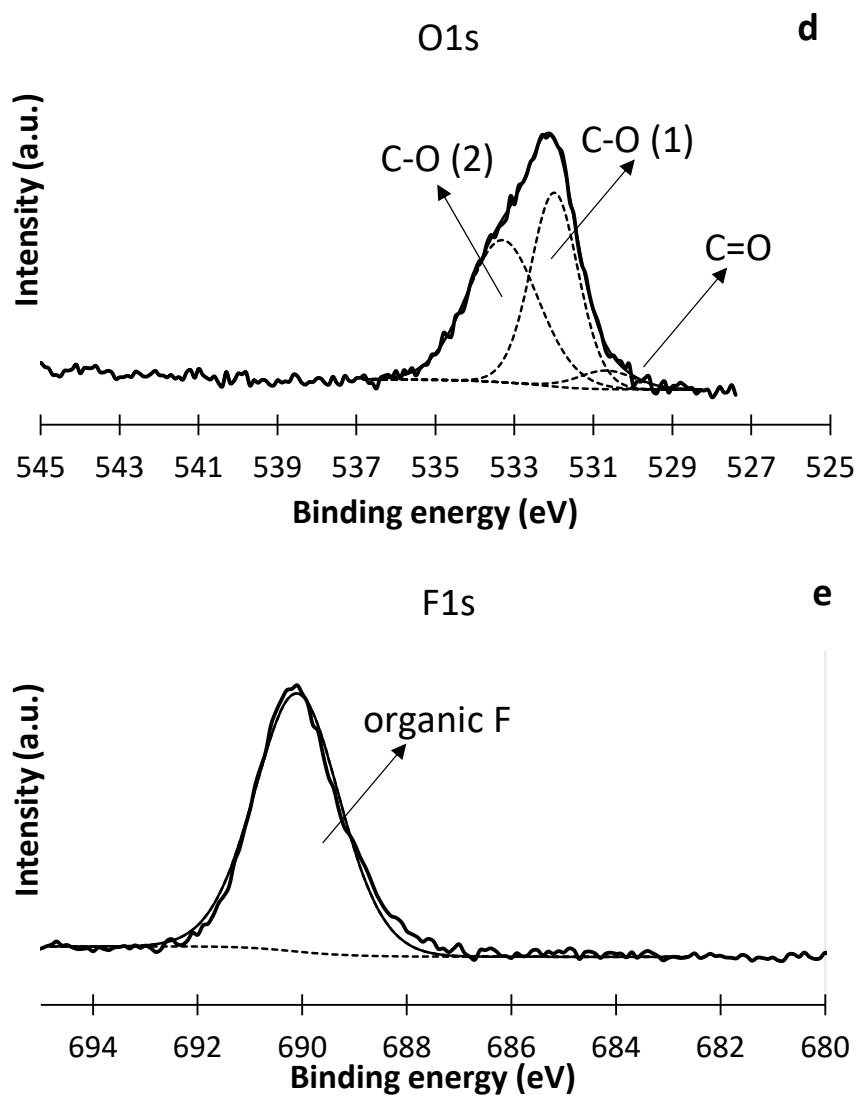
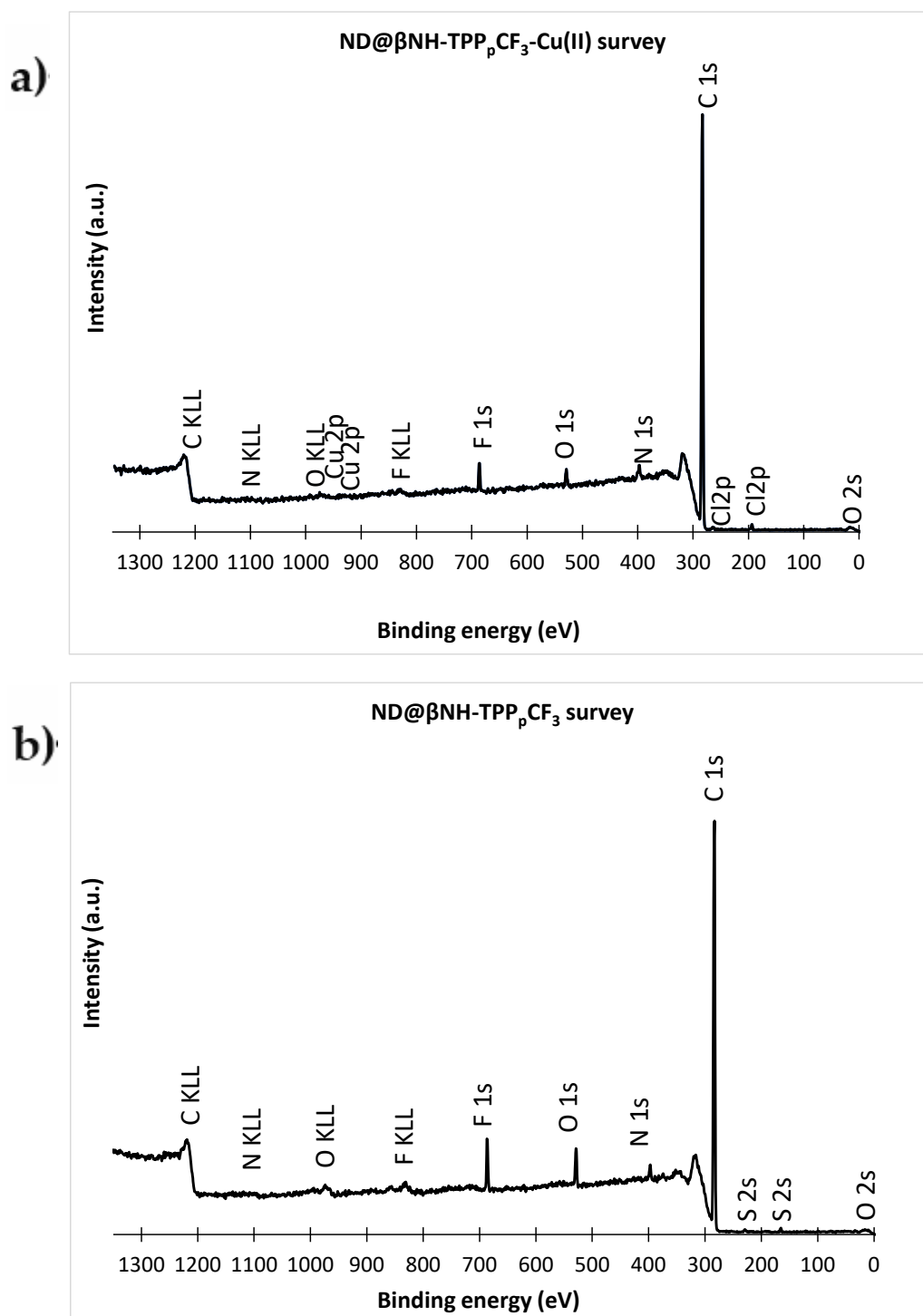


Figure S2. XPS results of hybrid sample ND@ $\beta$ NH-TPPpCF<sub>3</sub>: C1s (a,b), N1s (c), O1s (d), F1s (e).



**Figure S3.** Survey XPS spectra of ND@βNH-TPP<sub>p</sub>CF<sub>3</sub>-Cu(II) (a) and ND@βNH-TPP<sub>p</sub>CF<sub>3</sub> (b).

In all thermograms, one endothermic peak at 50 °C–150 °C was observed, which can be attributed to the weight loss caused by adsorbed water/solvents. In the ND@NH<sub>2</sub> thermogram (Figure S3a), an additional 3.5% weight loss was observed, attributed to decomposition of the 2-aminoethyl-acetamide groups linked to the surface of the ND (0.64% of NH<sub>2</sub>, corresponding to 0.39 mmol/g). In the thermograms related to ND@βNH-TPP<sub>p</sub>CF<sub>3</sub>-Cu(II) and ND@βNH-TPP<sub>p</sub>CF<sub>3</sub> (Figure S3b and S3c, respectively), exothermic peaks between 200 °C and 780 °C were observed, arising from decomposition of nitro-porphyrins **1** or **2**, resulting in weight losses of 9.1% and 9.8%, respectively.

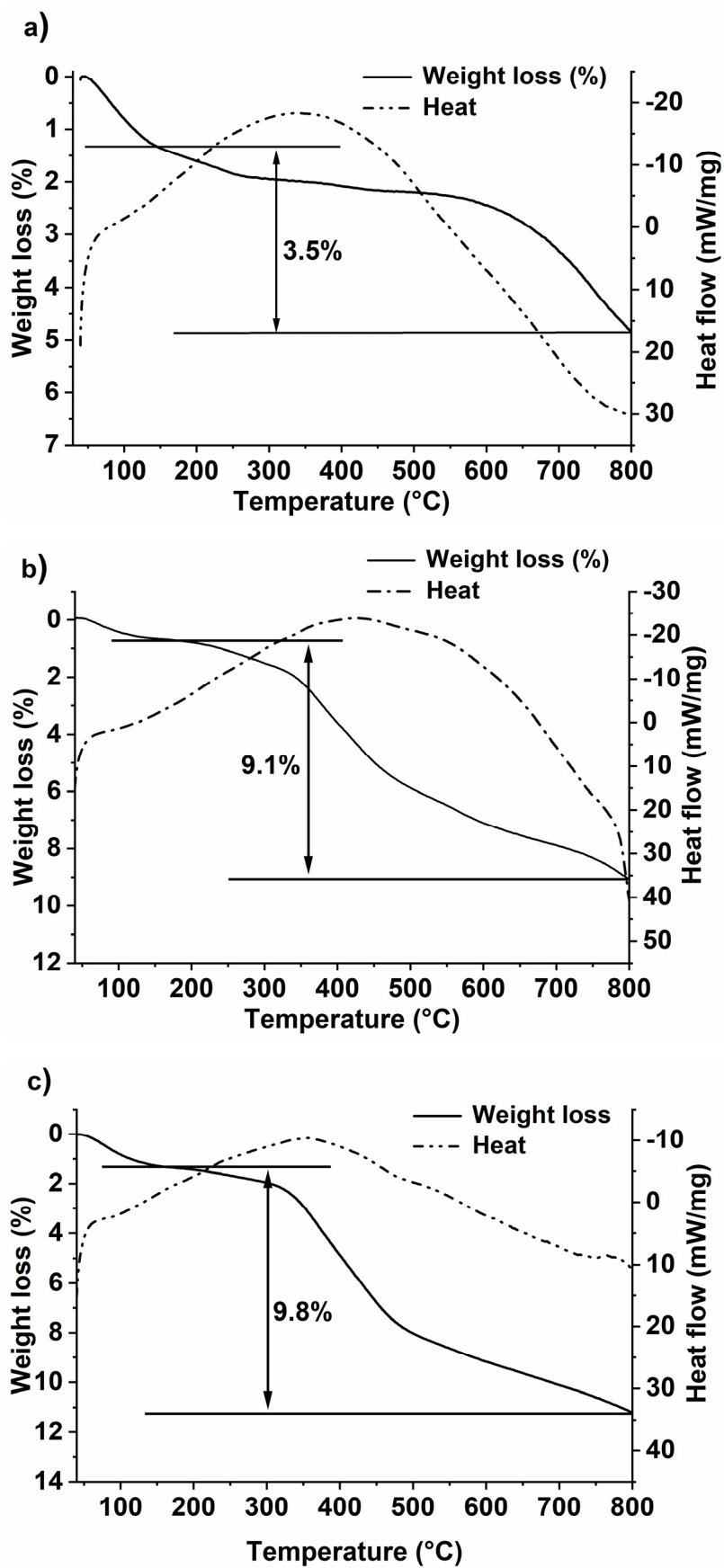
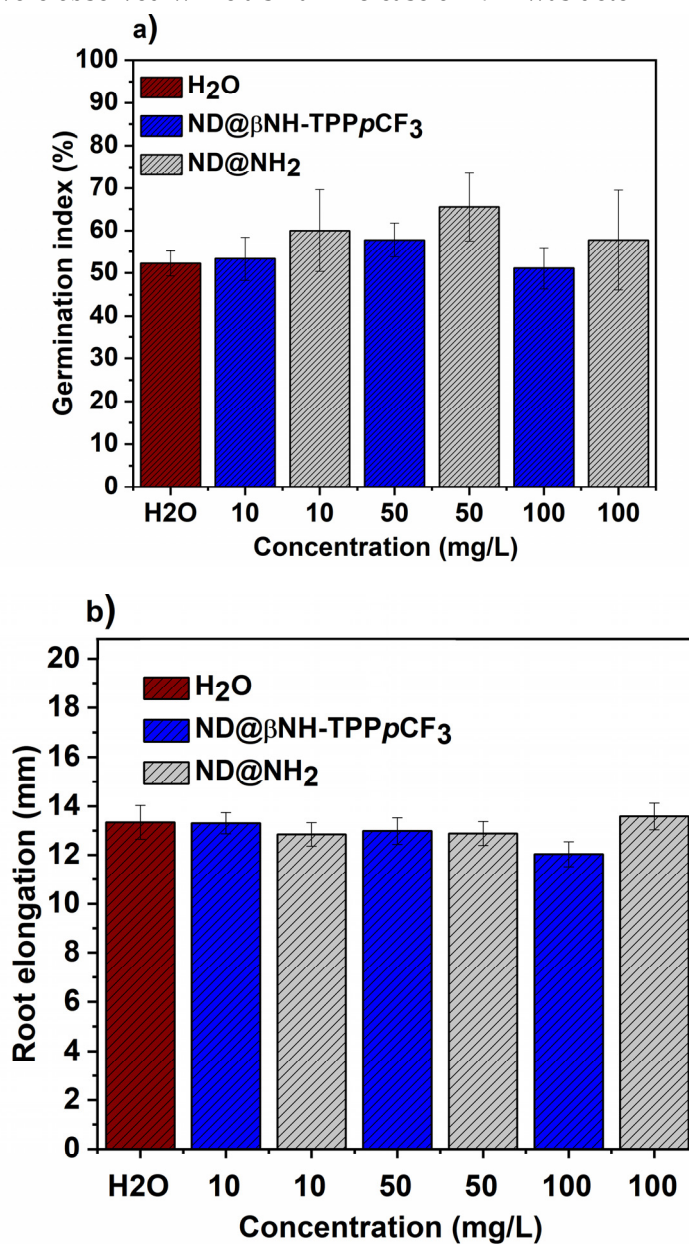
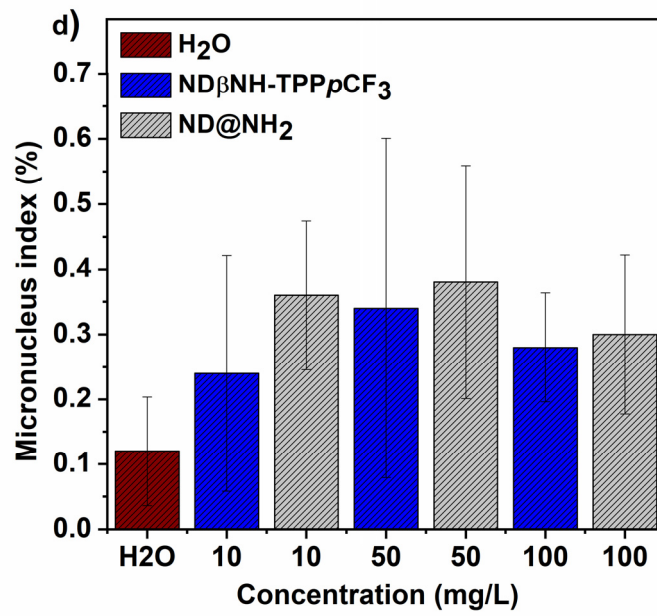
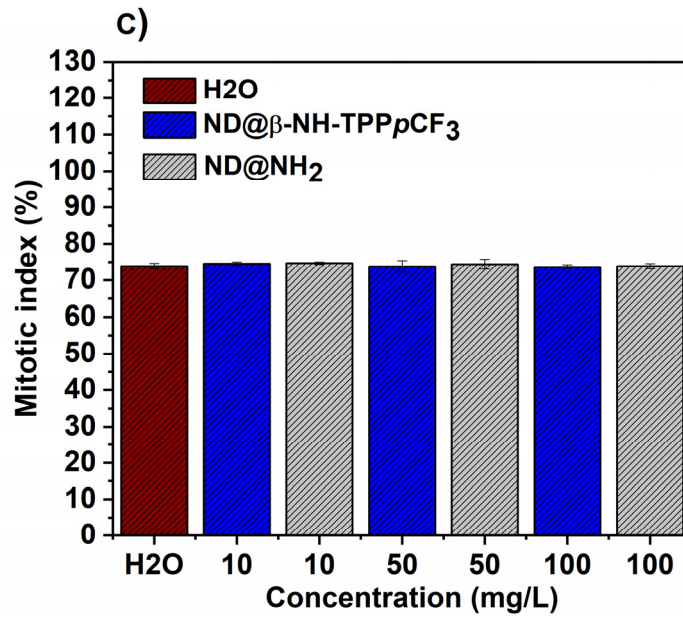
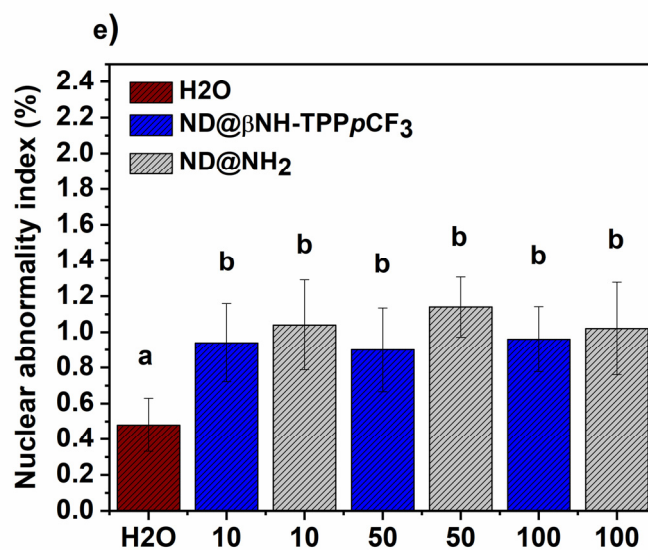


Figure S4. TG-DSC curves of: a) ND@NH<sub>2</sub>; b) ND@βNH-TPPpCF<sub>3</sub>-Cu(II); c) ND@βNH-TPPpCF<sub>3</sub>; weight loss (solid line); heat flow (dashed line).

A cytotoxic and genotoxic evaluation of  $\text{ND@NH}_2$  and  $\text{ND@}\beta\text{NH-TPPpCF}_3$  using *Allium cepa* as plant model was carried out (Figure S5). The phytotoxic effects were investigated by monitoring germination (GI) and root elongation (REI) indexes (Figures S4a,b). The cytotoxic potential was evaluated by mitotic index (MI) while the genotoxic effects were determined by analyzing micronucleus (MNI) and nuclear abnormality (NAI) indexes (Figures S4c–e). *Allium cepa* seeds (30 seeds per sample) were exposed to three concentrations (10, 50, and 100 mg/L) of amine-functionalized nanodiamond ( $\text{ND@NH}_2$ ) and nanodiamond porphyrin-functionalized on its surface ( $\text{ND@}\beta\text{NH-TPPpCF}_3$ ). A control group was also investigated in which seeds were submitted to  $\text{H}_2\text{O}$ . Results demonstrated that both  $\text{ND@NH}_2$  and  $\text{ND@}\beta\text{NH-TPPpCF}_3$  were not phytotoxic, nor cytotoxic, even when tested at a high concentration (100 mg/L) as no statistical differences in GI, REI, and MI were observed when compared to the control group. In addition, the data also revealed that  $\text{ND@NH}_2$  and  $\text{ND@}\beta\text{NH-TPPpCF}_3$  presented a very low genotoxic potential as no significant changes on MNI were observed while a small increase of NAI was determined.







**Figure S5.** Effect of the ND@NH<sub>2</sub>, ND@βNH-TPPpCF<sub>3</sub> and H<sub>2</sub>O (control group) on (a) the germination index (GI); (b) the root elongation index (REI); (c) the mitotic index; (d) the micronucleus index; (e) nuclear abnormality index.

## References

- Holt, K.B.; Caruana, D.J.; Millan-Barrios, E.J. Electrochemistry of Undoped Diamond Nanoparticles: Accessing Surface Redox States. *J. Am. Chem. Soc.* **2009**, *131*, 11272–+, doi:10.1021/ja902216n.
- Dhanak, V.R.; Butenko, Y.V.; Brieva, A.C.; Coxon, P.R.; Alves, L.; Siller, L. Chemical Functionalization of Nanodiamond by Amino Groups: An X-Ray Photoelectron Spectroscopy Study. *J. Nanosci. Nanotechnol.* **2012**, *12*, 3084–3090, doi:10.1166/jnn.2012.4547.
- Pastrana-Martinez, L.M.; Morales-Torres, S.; Carabineiro, S.A.C.; Buijnsters, J.G.; Figueiredo, J.L.; Silva, A.M.T.; Faria, J.L. Photocatalytic activity of functionalized nanodiamond-TiO<sub>2</sub> composites towards water pollutants degradation under UV/Vis irradiation. *Appl. Surf. Sci.* **2018**, *458*, 839–848, doi:10.1016/j.apsusc.2018.07.102.
- Turner, N.H. X-ray photoelectron and Auger electron spectroscopy (Reprinted from Analytical Instrumentation Handbook, Second Edition, Revised and Expanded, pg 863, 1997). *Appl. Spectrosc. Rev.* **2000**, *35*, 203–254, doi:10.1081/asr-100101225.
- Kirman, A.R.; Peng, W.; Mahfouz, R.; Amassian, A.; Losovyj, Y.; Idriss, H.; Katsiev, K. On the relation between chemical composition and optical properties of detonation nanodiamonds. *Carbon* **2015**, *94*, 79–84, doi:10.1016/j.carbon.2015.06.038.
- Lykaki, M.; Pachatouridou, E.; Carabineiro, S.A.C.; Iliopoulou, E.; Andriopoulou, C.; Kallithrakas-Kontos, N.; Boghosian, S.; Konsolakis, M. Ceria nanoparticles shape effects on the structural defects and surface chemistry: Implications in CO oxidation by Cu/CeO<sub>2</sub> catalysts. *Appl. Catal. B-Environ.* **2018**, *230*, 18–28, doi:10.1016/j.apcatb.2018.02.035.

